Article:
Kim, G.B., Pilakoutas, K. and Waldron , P. (2008) Thin FRP/GFRC structural elements. Cement and Concrete Composites, 30 (2). pp. 122-137. ISSN: 0958-9465

Thin FRP / GFRC Structural Elements

*G.B. Kim[a], K. Pilakoutas[b], and P. Waldron [b]

[a] Ph.D. Candidate, Department of Civil & Structural Engineering, The University of Sheffield, Mappin Building, Mappin Street, Sheffield, S1 3JD, United Kingdom.

[b] Professor, Department of Civil & Structural Engineering, The University of Sheffield, Mappin Building, Mappin Street, Sheffield, S1 3JD, United Kingdom.

* Corresponding author: Tel. +44-114-2225729, Fax +44-114-2225700, Email cip01gk@sheffield.ac.uk

Date Written: **September 2005**

Number of Words: **144**

Number of Words: **5,414**

Number of Tables: **4**

Number of Figures: **20**

Abstract

This paper presents background work leading to the development of thin structural elements made of GFRC (Glass Fibre Reinforced Concrete) reinforced with FRP (Fiber Reinforced Polymer) bars. Such thin structural elements are suitable for a variety of applications such as cladding, security barriers, etc, but this paper focuses on their use as permanent formwork. The first part of the paper deals with optimising the GFRC section to achieve maximum flexural capacity at minimum weight. The second part deals with the interaction between FRP and GFRC, in particular with the issues of bond. The third part deals with the performance of a 3m span thin GFRC permanent formwork panel system reinforced with FRP. Both experimental and analytical studies are presented and it is concluded that FRP / GFRC thin structural elements can be designed using section analysis which requires the appropriate use of material characteristics.

Keywords: FRP, GFRC, thin structural elements, permanent formwork, bond stress - slip, skin and rib design

1. Introduction

Innovative, economical and efficient methods of construction are continuously being sought by the construction industry. One particular area where there is still a lot of scope for innovation is in the development of durable reinforced concrete (RC) thin structural elements. However, the problem with thin concrete structural elements is that, if unreinforced, they lack toughness and break easily during demoulding or transportation.

There are two main alternatives to this problem. The first is to use conventional steel reinforcement. However, the RC panel will then need to be at least 80mm thick due to the requirement to provide cover in the steel for durability purposes. The second alternative is to employ Glass Fibre Reinforced Concrete (GFRC) using short fiber

reinforcement such as Alkali Resistant glass fibres. This is already being used extensively in many non-structural architectural concrete applications with typical minimum thicknesses of 20–50 mm in which the panel is usually supported frequently on a structural frame. A combination of the two alternatives is possible as demonstrated by the hybrid permanent formwork developed for the large drainage system shown in Figure 1 which utilises the "skin and rib" design concept [1]. In this particular application the formwork has a primary structural function for only a short period of time as the channel is backfilled with in situ concrete and, hence, there are no durability concerns. When durability is a bigger issue (such as for cladding panels or bridge permanent formwork) FRP reinforcement could be used as an alternative to conventional steel reinforcement.

This paper deals with the development of thin concrete permanent formwork. The first section introduces the main types of permanent formwork used today and discusses their advantages and disadvantages. Following that a thin GFRC section is considered and an optimisation exercise is undertaken to minimise weight for a particular span. This helps to identify the span and maximum length of an unreinforced thin GFRC element. Naturally, the next step is to reinforce the GFRC with FRP. Since no previous work has been done in this field the initial investigations deal with the bond characteristics. Finally, a thin FRP reinforced GFRC panel is tested and the paper presents the results and analysis.

2. Permanent Formwork Systems

Currently, the three most common materials used in permanent formwork systems are steel, precast concrete, and GFRC (Figure 2). In the development of a new concept for permanent formwork, there are two major issues that need to be considered : (1) optimal

utilisation of the material (cost constraint), and (2) achieving longer unsupported spans (technological constraint).

In the UK, steel decking is the most common permanent formwork system, especially for multi-storey steel framed building construction, because it is light and easy to install. Once in place, it requires very little additional connection to the frame and only small amounts of additional bar reinforcement. There are, however, a number of disadvantages with this system: (i) the profile of the decking is rolled from a steel sheet of constant thickness, which does not necessarily lead to the optimal utilisation of the material; (ii) it spans in one direction only, which limits the unsupported span length; (iii) the steel is not placed in the optimal position so the strength of the steel is not fully utilised once the concrete hardens and composite action is established; and (iv) all steel structures must also be protected against fire which adds significantly to the cost if special finishes are required.

Precast concrete systems often offer an attractive and economic alternative to metal decking by eliminating the need for fireproofing and any additional finishes for durability. Nevertheless, due to the weight of such units, mechanised handling is generally required. In addition, a topping layer of concrete is needed to tie the concrete planks together. These can complicate and add cost to the installation.

The truss-plank type of formwork (Figure 2(c)), which relies on a steel space truss partly embedded in a thin concrete slab, can span longer distances due to having an effective load carrying system in the form of a steel truss. This type of permanent formwork has potential economic advantages by providing speedy unpropped construction and excellent controlled surface finishes. However, due to the development of tensile strains induced in the precast concrete at the construction stage, the quality of

the surface can be affected by unsightly cracking. Strong connections are also required between the top and bottom chords because shear strength is critical at the supports.

Thin-walled GFRC is already commonly used for a range of small elements like channels, ducts and cladding panels, and, due to its light weight, has considerable potential in the development of new permanent formwork solutions. However, in order to deliver deflection control during construction, the overall depth of unsupported GFRC formwork would have to be increased because the stiffness of GFRC is not as high as that of steel.

Although the permanent formwork solutions mentioned above are relatively efficient in their use of materials, the basic cost of materials could be reduced further by introducing a new philosophy for design and optimisation. By adopting new materials, such as FRP and GFRC, it is possible to design new systems for permanent formwork for particular applications in the construction market. The first part of this paper deals with section optimisation issues.

3. Optimum cross section for a thin element as permanent formwork

The cost of permanent formwork is dominated by the amount of material used in its manufacture. As conventional metal decking is invariably made from steel sheet of constant thickness, the amount of material used is proportional to the total width of the strip from which it is formed. Figure 3 shows cross-sections and dimensions of typical profiles in common use.

In the following calculations, it is assumed that sections behave as normal thin walled beams. To reduce deflections in the formwork, the second moment of area of the section should be as large as possible. The second moment of area, I, and the weight of material per unit area, W_{ua}, of the trapezoidal section shown in Figure 3(a), are calculated using the formula given by Rockey and Evans [2]:

$$I = \frac{At^4}{6} + \frac{At^4}{2}\left[B\sin\theta - 1\right]^2 + \frac{t^4 B^3 \sin^2\theta}{6} \tag{1}$$

and

$$W_{ua} = \frac{(A+B)\rho t}{(A+B\cos\theta)} \tag{2}$$

where ρ is the density of the sheet material. The section modulus per unit weight of a given section is given by :

$$Z'_w = \left(I / y_m\right) \Big/ W_{ua} \tag{3}$$

where y_m is the distance from the bottom fibre to the neutral axis of the section.

The formulae in Eqs. (1) - (3) do not consider the possibility of buckling and are limited to an equal length of top and bottom plate. Because it is difficult to calculate the moment of inertia for any arbitrary cross section, previous research by Timoshenko [3], Hopkins [4], Lee et al [5], Chung [6], and Rajendran [7], has concentrated on standard approaches using the summation method to evaluate the general section properties. In order to investigate section properties of more complicated shapes, and in particular re-entrant sections, Equation (1) - (3) were modified by using an approximate method where the section is first discretized into a number of equal length segments. The moment of inertia for the sections shown in Figure 3(b) and (c), were calculated using Eq. (4) for re-entrant sections and Eqs. (5) - (7) for sinusoidal sections.

$$I = \frac{Dt^4}{6} + \frac{Dt^4}{2}\left[B\sin\theta - 1\right]^2 + \frac{t^4 B^3 \sin^2\theta}{6} + B^3 t^4 \sin^2\theta\cos\theta \tag{4}$$

$$I_x = \sum_{n=1}^{m} \Delta I_{xn} \tag{5}$$

$$\Delta I_{xn} = \frac{t_c(\Delta u)^3}{12}\sin^2\theta_n + t_c(\Delta u)\bar{y}^2 \tag{6}$$

$$\bar{y} = \frac{y_n + y_{n+1}}{2} \tag{7}$$

where *m* is the total number of segments; Δu is the constant segment length; and ΔI_{xn} is the moment of inertia of a segment above the centroidal axis.

After comparing sixteen different cross-sectional configurations having uniform thickness by Kim, et al. [8], the sinusoidal sections were shown to be the least efficient in terms of, the moment of inertia per metre width, I'_m, followed by the trapezoidal sections. The optimum solution is given by the re-entrant section which is almost twice as efficient as the sinusoidal section. An additional and consequential problem of the sinusoidal sections is that they are less able to control deflections. Kim, et al. (2004) showed that these sections would require support at centres less than 2m if the maximum deflection at the construction stage for a 200mm deep slab is to be maintained at less than 1/250 (=0.004) of the span between props. Deflection will also be the problem for GFRP sections under normal working loads and, hence additional reinforcement would be required since the strength of GFRP would not be utilized in such applications.

It can be concluded that GFRC sections of uniform thickness can be used as permanent formwork for moderate depths and spans, but will be limited in their range of applications by deflection and self-weight. Clearly, to increase the unsupported span, GFRC sections will need to be reinforced.

4. Proposal for new elements made of FRP reinforced GRFC

To avoid problems of durability associated with steel rebars with little cover, thin GFRC sections can be reinforced with FRP. This section examines the use of FRP reinforcement in thin GFRC sections designed using the "skin and rib" approach [1].

There are several issues to consider when dealing with FRP in GFRC sections : (i) the thickness of GFRC need not be constant; (ii) for practical purposes, the minimum thickness of GFRC has to be at least 5mm; and (iii) the controlling stress in GFRC is its

tensile strength since the compressive strength is much higher. Therefore, the FRP reinforcement should be added to the tensile region and the amount of GFRC below the neutral axis depth should be minimized to reduce weight. Two suitable sections proven by Kim, et al. [8] to be best in terms of deflection control and capacity, respectively, are shown in Figure 4.

The main design issues concerning the development of such permanent formwork include:

1) Bond. No previous studies have been reported on the interaction between GFRC & FRP, hence a comprehensive understanding of this interaction is required before the concept is accepted for further investigation.

2) Cover. GFRC is a good material for protecting reinforcement from the environment and FRP reinforcement does not require the same level of protection as conventional steel. Hence, the cover requirement can be relaxed provided that bond requirements can be meet.

3) Deflections. Since GFRC is not that much stiffer than glass FRP, it is necessary to increase the overall depth of its section to deliver better deflection control. Alternatively, the element will need to be pre-cambered, to counter some of the permanent deflection.

4) Crack widths. The crack width limit used in bridge structures, required for the protection of steel reinforcement, is normally less than 0.1mm. In the case of FRP reinforcement this limit may be relaxed up to 0.5mm by ACI 440.1R-01 [9].

5. Experimental Programme

The experimental work on bond deals with both direct pull-out tests and splitting pull-out tests. Standard pull-out tests are needed to determine the bond characteristics in well

confined conditions, whilst the splitting pull-out tests enable us to understand better the bond behaviour in thin flexural elements.

5.1 Manufacture of pull-out specimen

The GFRC was made from Type I Portland cement, sand, and chopped glass fibres of 15mm maximum length. Mix 1 and Mix 2 were designed with different volume fractions of fibres of 2% and 3%, respectively. The mix proportions were 0.35 : 1.0 : 1.0 (water : cement : sand) by weight. Concrete test cylinders 100 dia × 200mm (six for each GFRC mix) provided average compressive strengths, f_c' of 54 MPa (Mix 2 – 24 days) and 66 MPa (Mix 1 – 40 days), respectively. The average tensile strengths at the same age were determined to be 6 and 7 MPa, respectively, by using the Brazilian test on three additional cylinders. Each pull-out specimen was cast with either 8mm square Glass Fibre Reinforced Polymer (GFRP) bar, supplied by Eurocrete Ltd, (E=41GPa, strength=900MPa) having a rough surface provided by a peel ply or 6mm diameter high yield (460MPa) deformed steel bar. After casting, specimens were cured in 100 percent humidity at ambient laboratory temperature for 24 or 40 days prior to testing.

5.2 Test specimens, variables and procedures

The characteristics of the local bond stress-slip response of reinforcing bars in GFRC were investigated by conducting 12 standard pull-out tests and 12 splitting pull-out tests based on the international Round Robin Test [10] procedure for FRP bars in normal unreinforced concrete.

Three specimens from each group were tested using a 500 kN capacity universal testing machine, following the iRRT. Slip measurements were made using linear variable differential transducers (LVDTs) fixed on the surface of the cubes at both the loaded and free ends. Measurements of load and displacement were taken every 2 seconds by a computer controlled data acquisition system. Figure 5 shows details of the positioning of the bar in the concrete cube and loading frame for both the standard pull-out and

splitting pull-out tests. A schematic representation of the test setup, giving relevant dimensions, is shown in Figure 6.

5.3 Standard pull-out tests

In designing reinforced concrete members, it is assumed that no slippage will occur between the bar reinforcement and the concrete when load is applied. If the bond capacity between the two is exceeded, the concrete surrounding the reinforcement may crush or split permitting the embedded bar to slip. The strength of reinforcing bar-to-concrete bond is dependent upon a number of factors, with concrete compressive strength, reinforcing bar diameter and spacing, and embedment length being the most significant. Nominal bond strength is determined experimentally by the pull-out test, which basically involves measuring the force needed to produce measurable slippage or pull out of a bar embedded in concrete.

In the pull-out tests, the actual slip of the bar with respect to the concrete, δ_{le}, was calculated by subtracting the elastic elongation of the unbonded portion of the bar, Δl, from the average slip measurements of three LVDTs, δ_{av}, as shown in the following equations.

$$\delta_{av} = (\delta_1 + \delta_2 + \delta_3)/3 = \delta_{le} + \Delta l \tag{8}$$

$$\Delta l = Fl_a/(EA) \tag{9}$$

$$\delta_{le} = \delta_{av} - \Delta l = (\delta_1 + \delta_2 + \delta_3)/3 - Fl_a/(EA) \tag{10}$$

where δ_1 , δ_2 , δ_3 = slip measurements of the three LVDTs ; l_a is the unloaded length (see Figure 5); F is the applied pullout load; E represents the elastic modulus of the bar; and A is the cross-sectional area of the bar.

The value of nominal bond stress was calculated as the recorded pull-out resistance force on the bar divided by the nominal surface area of the embedment length of the bar with the assumption of uniform bond stress distribution along the embedded length, as

shown in equation (11). In all cases, pull-out failure (F) was defined as the point of maximum pull-out load.

$$\tau = \frac{F}{CL} \tag{11}$$

where C is the circumference (C = πd for round bars, C = 4d for square bar), d is the diameter and L is the bonded length of the bar.

5.4 Splitting pull-out test

The splitting test is designed to give a more representative measure of the bond strength when a bar, such as the ones shown in Figure 6, is near the boundary. In order to investigate the splitting behaviour of reinforcing bars in GFRC concrete, 12 further pull-out specimens were tested with the bar placed eccentrically following the same test procedure as for the pull-out test. The configuration of the specimens is shown in Figure 6. In the splitting test, the load and displacement values were used to calculate the corresponding nominal bond stress and slip in exactly the same way as for the standard pull-out test.

6. Experimental Results

A summary of all the test results is presented in Table 1. From the standard deviation values it is apparent that there is considerable variability in the test results, in particular for δ_{peak} .

6.1 Slip Characteristics

Typical slip characteristic curves can be seen in Figure 7 (a), for the standard pull-out test, and Figure 7 (b), for the splitting test which show results for the average slip of the loaded end, the slip of the free end and the difference between the two. It is clear that slip at the loaded end starts at a very early stage, but the free end only slips at around 70% of P_{max}. Hence, it appears that the debonding process is gradual, starting at the loaded end and spreading towards the free end. After initial free end slip, there is still

additional resistance up to P_{max}. At this load δ_{peak} comprises slip due to rigid body movement of the entire bar and slip associated with the cumulative deformation of the bar along the embedded length. In Figure 7(a), curve 3 shows the net extension of the embedded length. At P_{max}, the rigid body deformations are small enough to be the result of deformation of the resin rich layer of the bar surface.

Soon after P_{max}, the resin rich layer of the surface appears to fail abruptly and the bar pulls-out by several millimetres. The bar then locks again and frictional resistance results in relatively good residual bond stress (around 43% of τ_{max}).

In the case of the splitting test, slip again begins at the loaded end. However, this time bond failure occurs as a result of concrete splitting, as shown by the crack width measurements in figure 7(b) (curve 4). The maximum bond stress is only about 27% of τ_{max}. This value depends not only on the depth of the cover, but also on the bar surface and concrete cover characteristics.

6.2 Comparison between GFRC and plain concrete with embedded FRP reinforcement

Representative bond stress–slip curves for 8mm GFRP bars in GFRC and concrete are shown in Figure 8. Kim et al. [11] suggest from the Pull-out test results that the bond strength of the GFRP reinforcing bar to GFRC is approximately 1.6 times that to plain concrete. As seen in Figures 8 (a) & (b) the bond–slip characteristics of the GFRP bars in the two materials are very similar. However, GFRC not only gives higher initial strength but also higher residual strength. The splitting bond stress is also about 26% higher in GFRC than in concrete, although the failure mechanism is the same.

6.3 Comparison of Steel & GFRP bar

From Figure 9 (a) & (b), it can be seen that steel reinforcement achieves much higher pull-out and splitting strengths than the FRP bars. This may be partly attributed to the fact that the steel bar diameter is smaller, having only 56 % of the area of the FRP bar. However, from Figure 9 (a), it can be seen that the failure mode is somewhat different

from that for FRP, since initial slippage occurs suddenly and most likely without any damage to the steel bar surface.

6.4 Comparison of Mix1 & Mix2

Figures 10 (a) - (d) show the results of bond stress versus slip for 6mm steel and 8mm GFRP bars for two different mixes of GFRC. In the standard pull-out tests, the bond strength for Mix 1 with the lower amount of fibre reinforcement is higher than for Mix 2 both for steel and FRP, but with very similar overall characteristics. It appears that the higher compressive and tensile strength associated with Mix 1 due to its greater age at the time of testing is more important than the lower percentage of glass fibre it contained. This is surprising, since more fibre reinforcement in GFRC is expected to provide higher tensile resistance to the splitting crack and lead to higher bond stresses in the splitting test. Further investigations are needed to examine this effect further.

From the bond tests it can be concluded that, due to improved bond characteristics, it is possible to design FRP GFRC elements with reduced cover requirements. Now that this has been established, thin GFRC elements with FRP reinforcement will be examined further in the following section.

7. Analysis of FRP reinforced GFRC

To enable direct comparisons to be made with the work on GFRC cross sections presented earlier, the same basic dimensions of the elements have been adopted here. This means that the depth of the unit has been kept at 110mm and the thickness of the GFRC generally maintained at 10mm. A cover of 10mm all around the FRP bar has also been assumed. The FRP bar used as reinforcement is an 8mm square GFRP bar having elastic modulus E = 41 GPa and strength around 900 MPa. Typical cross sections for section types M13 and M5, taken from Kim, et al. [8], are shown in Figure 11.

To simplify the problem, the following are some of the assumptions adopted for the purposes of this section analysis.

1. Plane sections remain plane after bending, i.e. a linear strain distribution is assumed through the cross section.
2. There is perfect bond between the GFRC and the reinforcing FRP bars.
3. No tensile stress is carried by the concrete below the neutral axis.
4. GFRC behaves in compression like conventionally reinforced concrete.

The dead (D) and live (L) ultimate load combination used in BS8110 [12] is 1.4 D + 1.6 L. This leads to a design ultimate load of 10.8 kN/m^2 which has been used to calculate the corresponding stress in the GFRP bar. Figures 12 and 14 compare the stress in the GFRP rebar for different span lengths and for various element widths (W) ranging from 200 - 368 mm and 120 - 360 mm, for section type M13 and M5, respectively. It shows, as expected, that the smaller the width, the lower the stress in the GFRP rebar. In terms of capacity, the maximum span length for such permanent formwork is almost 4m. As can be seen from Figure 13 dealing with normalised deflection and capacity, for a similar unreinforced section (in case of W = 250mm, section type M13) with a GFRC strength of 6 MPa, the maximum span length is just over 1m. On the other hand, for section type M5 in Figure 15 (W = 300mm), the span lengths of up to 3m can be achieved.

Though the increase in capacity is spectacular the deflections and crack widths need to be examined as well. At the moment there are no design recommendations of GFRC reinforced with FRP so the recommendations by ACI committee 440 [9] for FRP reinforced concrete have been used. As far as deflections and cracking are concerned the ACI proposes the following equations (12) – (14) for deflection, δ , the effective moment of inertia on cracked section, $I_{cr,e}$, and crack widths in FRP reinforced members, ω , respectively.

$$\delta = \frac{5wL^4}{384EI} \text{ for distributed load, } \delta = \frac{Ps}{48EI}\left(3L^2 - 4s^2\right) \text{ for four point load} \qquad (12)$$

where w is the distributed load, P is the total service concentrated load divided into two concentrated load P/2 each applied at a distance s from the support, and L, E and I are the span length, elastic modulus and second moment of the bar respectively.

$$I_{cr,e} = \left(\frac{M_{cr}}{M_a}\right)^3 \beta_d I_g + \left[1 - \left(\frac{M_{cr}}{M_a}\right)^3\right] I_{cr} \leq I_g \tag{13}$$

where M_{cr} is the cracking moment, M_a is the applied moment and Reduction coefficient, $\beta_d = \alpha_b \left[\frac{E_f}{E_s} + 1\right]$, ($\alpha_b$ = bond dependent coefficient; E_f, E_s = modulus of elasticity of fiber and steel, respectively), and I_g is the gross moment of inertia, and I_{cr} is the moment of inertia of transformed cracked section.

$$\omega = \frac{2.2}{E_f} \beta k_b f_f \sqrt[3]{d_c A} \tag{14}$$

where β is the ratio of the distance from the neutral axis to the extreme tension fibre to the distance from the neutral axis to the centre of the tensile reinforcement, k_b is the bond-dependent coefficient, f_f is the stress in the FRP reinforcement in tension, d_c is the thickness of the concrete cover measured from extreme tension fibre to the centre of the bar, and A is the effective tension area of concrete, defined as the area of concrete having the same centroid as that of tensile reinforcement, divided by the number of bars. Equation (13) is only valid for $M_a > M_{cr}$. The factors α_b and k_b reflect the weaker bond characteristics of some FRP bars. However, from the reported tests on the bond characteristics, the authors consider that these factors are unnecessary for FRP bars embedded in GFRC. The modified equations were used to determine the deflections and crack widths for the FRP reinforced GFRC section shown in Figure 16. It is evident, that even though the capacity of this section is adequate for spans of up to 4m, at that span it would exceed both the deflection and crack width limits. In fact, type M13 section is only capable of spanning 2.60m before the crack width limit of 0.5mm is exceeded and 2.60m before it exceeds the deflection limit of L/250. For the type M5

section, the maximum span is just 2.55m and 2.7m in terms of the crack width and deflection limits, respectively. But, the latter section needs more concrete volume (5 times more) than type M13 and, hence, is less economic.

There are three main options to increasing the performance of the section with regard to deflection and crack width.

a) decrease the strain in the FRP bar by increasing the amount of reinforcement
b) increase the depth of the cross-section
c) provide an intermediate support

To predict the shear capacity, ACI Committee 440 [9] equation (15) and RILEM TC 162 [13] equations (16) – (19) are used.

$$V_c = \frac{\rho_f E_f}{90\beta_1 f_c'}\left(\frac{\sqrt{f_c'}b_w d}{6}\right) \tag{15}$$

Where ρ_f = flexural reinforcement ratio, E_f = modulus of elasticity of the FRP, β_1 = factor for concrete strength, f_c' = compressive strength of concrete, b_w = width of the web, and d = distance from extreme compression fibre to centroid of tension reinforcement.

$$V_c = V_{cd} + V_{fd} + V_{wd} \tag{16}$$

$$V_{cd} = \left[0.12k\left(100\rho_1 f_{ck}\right)^{1/3} + 0.15\sigma_{cp}\right]\cdot b_w d \tag{17}$$

Where $k = 1 + \sqrt{\frac{200}{d}} \le 2$, $\rho_1 = \frac{A_s}{b_w d} \le 2\%$, A_s = area of tension reinforcement, b_w = minimum width of the section over the effective depth, $\sigma_{cp} = \frac{N_{sd}}{A_c}$, and N_{sd} =longitudinal force in section

$$V_{fd} = 0.7k_f k_l \tau_{fd} b_w d \tag{18}$$

Where $k_f = 1 + n\left(\frac{h_f}{b_w}\right)\left(\frac{h_f}{d}\right) \le 1.5$, h_f = height of the flanges, b_f= width of the flanges, b_w = width of the web, $n = \frac{b_f - b_w}{h_f} \le 3$, $k_l = 1 + \sqrt{\frac{200}{d}} \le 2$, and $\tau_{fd} = 0.12 f_{RK,4}$

$$V_{wd} = \frac{A_{sw}}{s} 0.9 d f_{ywd} (1 + \cot\alpha) \sin\alpha \tag{19}$$

where s = spacing between the shear reinforcement measured along the longitudinal axis, α = angle of the shear reinforcement with the longitudinal axis, and f_{ywd} = design yield strength of the shear reinforcement.

8. Overall system of FRP reinforced GFRC

8.1 Experimental analysis

To validate the design assumptions, two GFRC panels (Type M13) reinforced with GFRP were manufactured for experimental testing as shown in Figure 17. These panels (L30G3, L30G2) were 3000mm long provided with 8mm square GFRP rebars and were reinforced with 3% and 2% of chopped glass fibre, respectively. The concrete mix used in the analysis is given in Table 2. The average compressive strength of GFRC, obtained by testing 100mm cubes in British Standard [14] at 28 days after casting, was 61.4 MPa and 69.8MPa for L30G3, L30G2, respectively. The average splitting tensile strength of cylindrical specimens, determined by splitting tests on 150 mm diameter x 300 mm long cylinders in British Standard [15] at 28 days after casting, was 7.0 MPa and 6.2MPa for L30G3, L30G2, respectively.

The panels were tested simply supported over a span of 2880mm, and loaded by two concentrated line loads placed at equal distance from the support (960 mm for L30G3 and 740 mm for L30G2), as shown in Figure 18. Displacement measurements were taken by LVDTs, at location indicated in Figure 18. The load was applied at a slow pace (initially 1 kN/min) by means of hydraulic jack in displacement control. Deflection and load values were monitored by means of a data acquisition system.

L30G3 was tested monotonically to failure. Failure occurred due to shear in the webs located in the shear span. The shear cracks were visible and opened widely before failure, hence though failure was abrupt it was not unexpected. After observing the fibre distribution along the failure surface of L30G3, it was noticed the direction of casting may have influenced the fibre orientation. Hence, it was decided to reduce the shear span for L30G2, so as to amplify the shear load in the shear span. It was also decided to apply a load cycle just after cracking and a load cycle at 8 kN. Figure 19 shows the large deflection achieved during loading as well as the cracks developed in the central region. Cracking started in the pure bending moment zone, but as the load was increased, shear stress induced inclined cracks to failure.

8.2 Discussion of results

a) Load - deflection

The load deflection curves for both specimens are shown in Figure 20(a). The figure also shows the load deflection curve predicted by the ACI 440 equation (13). The predicted curves are exceptionally good and demonstrate that the ACI deflection equations are also appropriate for thin GFRC reinforced FRP. To enable a better comparison between the two specimens, the moment resistance versus normalised deflection curves are shown in Figure 20(b). The deflections are normalised to eliminate the difference in the position of the load. As it can be seen, there are no major differences in the deflection response between L30G3 and L30G2 even though they have a different amount of glass fibre reinforcement. Furthermore, there was no evidence of bond slip between GFRP and GFRC which confirms that thin concrete elements can be achieved if the concrete is reinforced with fibres.

b) Flexural capacity

The flexural capacity of the panels can be estimated by using the ACI440 equation or simple section analysis (SA1). The predictions from these two approaches are shown in

Table 3, together with the experimented results. It is evident that these approaches underestimate the flexural capacity. Hence, a more sophisticated section analysis was undertaken, first by taking into account the stress-strain characteristics for GRFC in compression as measured from experiments (SA2) and by using the stress-strain potential in the tensile region of GFRC (SA3). The results from these analyses are also shown in Table 3. Since the specimens failed in shear, it can be assumed that their full flexural capacity is higher than achieved experimentally. That means that only SA3 predicts the capacity adequately. To confirm the validity of this analysis, the strains in the flexural reinforcement at the failure load obtained in the experiments was calculated and is shown in the table in parentheses. These predictions are close to the experimental values, and hence confirm that this type of analysis is appropriate for FRP reinforced GFRC.

c) Shear capacity

The determination of the shear capacity of thin concrete sections is not easy since there are no codes of practice or recommendations dealing with such elements. Hence the shear capacity is predicted by first assuming that only the web is effective in resisting shear (web only) and then an equivalent rectangular section is considered (transformed). Initially, the ACI 440 equation (15) for FRP RC are used as shown in Table 4, but the results are very conservative. Then the equations (16) – (19) for GFRC proposed by RILEM TC 162 [13] are used. Here, the equations are modified to account for the FRP reinforcement by multiplying the reinforcement ratio by E_{FRP} / E_{steel}. This approach is used extensively in European recommendations for FRP RC design guidelines - European Committee for Standardization [16] and Institution of Structural Engineers [17]. The RILEM approach appears to be more suitable for thin FRP reinforced GFRC, even though the results are still very conservative for the case of L30G3. It should be noted that L30G3 failed due a horizontal crack developing just above the flexural

reinforcement in the web. This mode of failure is not usually found in RC elements and may require a more direct check in thin GFRC elements.

10. Conclusions

Pull-out tests showed that the bond between the GFRP reinforcement and GFRC was approximately 60% greater than that for GFRP reinforcing bars embedded in plain concrete. Based on the results of these tests, the local bond stress–slip relationships predicted bond failure by pull-out and the volume of glass fibres in the GFRC matrix appeared to have no effect on the maximum bond strength and bond–slip response and practically no influence on the splitting bond resistance. It is concluded that thin GFRC element can be developed with GFRP reinforcement.

Equations for the optimum design of uniform thickness GFRC sections have been developed for use of these sections as permanent formwork.

FRP reinforced GFRC sections have a higher capacity than GFRC sections, but unpropped span lengths are restricted by the occurrence of large deflections and crack widths.

In order to predict the actual service load deflection based on the experimental results, simple empirical methods such as using the modified ACI 440 code were shown to be very accurate.

In terms of capacity, FRP / GFRC thin structural elements can be designed using a more sophisticated section analysis (SA3) that considers the stress-strain characteristics of GFRC in tension and compression. In terms of shear capacity, the RILEM recommendation, modified to account for FRP, were shown to offer the least conservative estimates of resistance, but further research is required to determine the web shear resistance.

References

1. Pilakoutas, K. and Petkovski, M. The Development of the Decathlon Drainage Channels, *Proceedings of the 12th International Congress or the International Glassfibre Reinforced Concrete Association*, Dublin, 2001, p. 3-11.
2. Rockey, K.C. and Evans, H.R. The behaviour of corrugated flooring systems, *Thin Walled Steel Structures – Their Design and Use in Buildings*, Symposium at University College of Swansea, September 11-14, 1969, p. 236-257.
3. Timoshenko, S.P. *Theory of plates and shells*, McGraw-Hill, 1959.
4. Hopkins, R.B. *Design Analysis of Shafts and Beams*, McGraw-Hill, 1970.
5. Lee, C.L., Mioduchowski A., and Faulkner, M.G. Opimization of Corrugated Claddings, *Journal of Structural Engineering*, August, 1995, p. 1190-1196.
6. Chung, K.F. The State-of-the-Art of Section Property Calculation of Structural Members with Arbitrary Shape, *J. Construct. Steel Research*, 32, 1995, p. 127–141.
7. Rajendran, S. A Fortran Program For Computing the Geometric Properties of Plane Lamina and Axi-symmetric Bodies, *Computers & Structures*, 54(5), 1995, p. 859–863.
8. Kim G.B., Waldron P. and Pilakoutas K. Applications of FRP/GRC in permanent formwork, *Proceedings of the first international conference on innovative materials and technologies for construction and restoration*, Lecce - Italy, June 6th ~ 9th, 2004, ed. by A. La Tegola and A. Nanni, pub. by Linguori Editore, Vol.1, pp 589-600, ISBN 88-207-3678-8.
9. ACI 440.1R-01. Guide for the Design and Construction of Concrete Reinforced with FRP Bars, *American Concrete Institute*, Farmington Hills, Michigan, 2001.
10. iRRT. *International Round Robin Test for FRP reinforcement*, <http://www.shef.ac.uk/~tmrnet/rrt>, Sheffield, 2002.

11. Kim, G.B., Waldron, P., and Pilakoutas K. Bond Behaviour of Reinforcing bars in GFRC, *Proceedings of the 13th Congress of the International Glassfibre Reinforced Concrete Association*, Barcelona, Spain, October 6^{th}~8^{th} , 2003.

12. British Standards Institution, BS8110. Part 1:Code of practice for design and construction, *British Standards Institution*, London, 1997.

13. RILEM TC 162-TDF. Test and design methods for steel fibre reinforced concrete, $\sigma-\varepsilon$ desing method ; final recommendation, Materials and Structures, Vol.36, October 2003, p.560-567.

14. British Standards Institution, BS1881-116. Part 116 : Method for determination of compressive strength of concrete cubes, *British Standards Institution*, London, 1983.

15. British Standards Institution, BS1881-117. Part 117 : Method for determination of tensile splitting strength, *British Standards Institution*, London, 1983.

16. European Committee for Standardization. Eurocode 2: Design of Concrete Structures - Part 1: General Rules and Rules for Buildings, prEN 1992-1 (1st draft), CEN, 1999.

17. Institution of Structural Engineers. Interim guidance on the design of reinforced concrete structures using fibre composite reinforcement, IStructE, SETO Ltd, London, 1999.

18. Mischopoulos, N. *Bond of FRP reinforcing bars in concrete – International Round Robin Tests*, Msc Dissertation, Dept. of Civil and Structural Eng., The University of Sheffield, 2001.

LIST OF TABLES

Table 1. Summary of the tests results

Series	Specimen notations	Measured Maximum load, $P_{max\_average}$ (kN)	Bond strength, $\tau_{max\_average}$ (MPa)	Standard Deviation, σ_τ (MPa)	Slip at P_{max}, $\delta_{peak\_average}$ (mm)	Standard Deviation, σ_δ (mm)	Crack width at 85% of P_{max}, $w_{max\_average}$(mm)
I	M1P6	15.9	28.2	1.14	2.99	2.26	-
	M12*	36.8	16.3	-	1.44	-	
II	M1P8	18.2	14.2	1.38	1.40	0.11	-
	M8*	10.8	8.5	-	0.82	-	
III	M1S6	4.3	7.7	2.16	0.41	0.07	0.005
	M12*	8.1	3.6	-	0.08	-	0.500
IV	M1S8	5.0	3.9	0.46	0.88	0.17	0.004
	M8*	4.0	3.1	-	0.03	-	0.027
V	M2P6	14.0	24.8	3.39	2.23	1.91	-
VI	M2P8	14.1	11.0	1.09	0.72	0.64	-
VII	M2S6	2.8	4.9	0.84	0.48	0.12	0.001
VIII	M2S8	4.9	3.8	1.30	0.25	0.06	0.001

* by Mischopoulos [18]

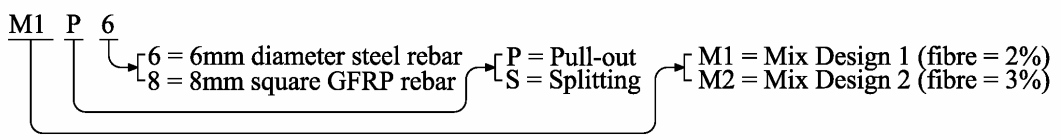

Table 2. Proportions of GFRC mixtures in kg/m^3

Mix Code	Cement OPC	Fibre Glass	Water	W/C	Aggregate Sand (#2 Sieve)	Super-plasticizer	Volume Glass contents(%)	PFA
L30G3	52.5	3.15	19.71	0.375	52.5	1.21	3	21.0
L30G2	52.5	2.10	19.71	0.375	52.5	1.21	2	21.0

Table 3. Measured and calculated ultimate load and strain in reinforcement

	Ultimate load, P_n (kN)					Strain in reinforcement (mm)			
	Exp.	ACI 440	SA1	SA2	SA3	Exp.	SA1	SA2	SA3
L30G3	8.7	8.3	8.4	9.2	10.3	0.0103	0.0146	0.0159	0.0136 (0.0107)
L30G2	13.4	11.0	11.9	13.3	14.7	0.0112	0.0156	0.0176	0.0153 (0.0133)

Notes) SA1 – Concrete no tension, SA2 – GFRC no tension, SA3 – GFRC with tension

Table 4. Measured and calculated shear capacity

	Exp.	ACI 440		RILEM TC162			
		(web only)	(transformed)	(web only)		(transformed)	
				Con.	Fibre	Con.	Fibre
L30G3	4.3	0.8	1.6	1.8	0.6	2.6	1.2
L30G2	6.7	0.7	1.5	2.0	0.6	2.8	1.2

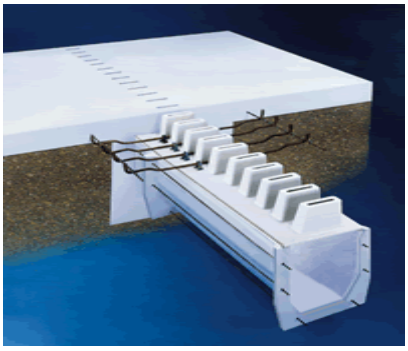

Figure 1. GFRC drainage channel permanent formwork systems (Courtesy Hodkin & Jones Ltd, UK)

(a) Steel decking

(b) Pre-cast concrete hollow slabs

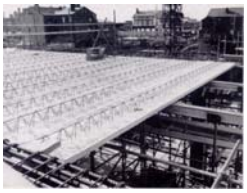

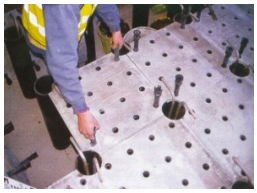

(c) Pre-cast (Truss-plank) (d) GFRC

Figure 2. Existing permanent formwork systems

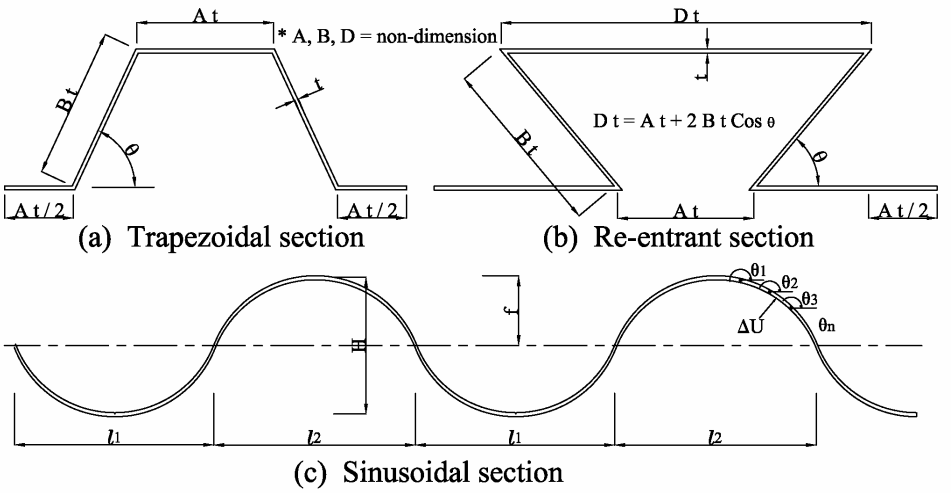

Figure 3. The dimensions of single profiles from typical sections

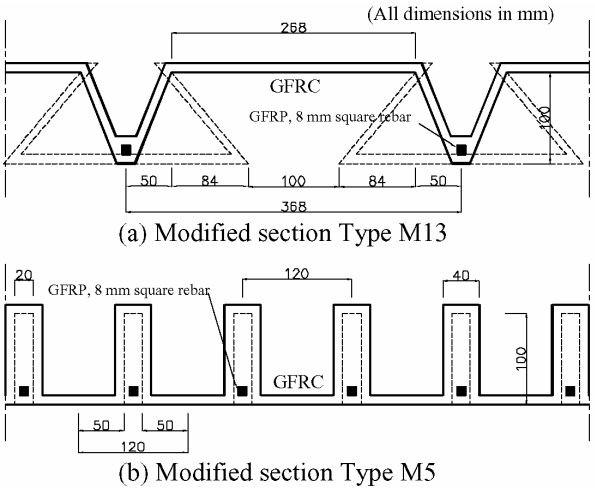

Figure 4. FRP reinforced GFRC panels

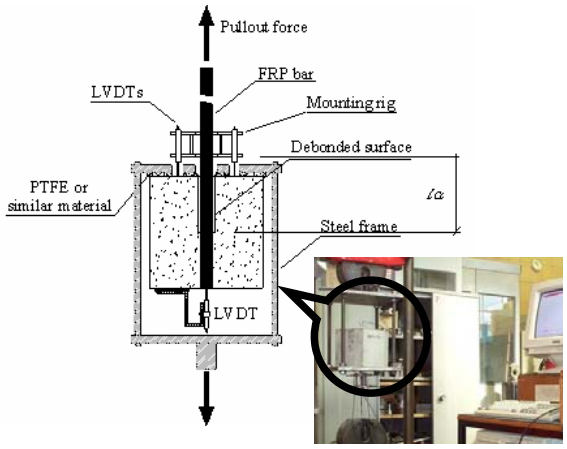

Figure 5. Details of the positioning of the bar and LVDT's in the GFRC specimen and loading frame.

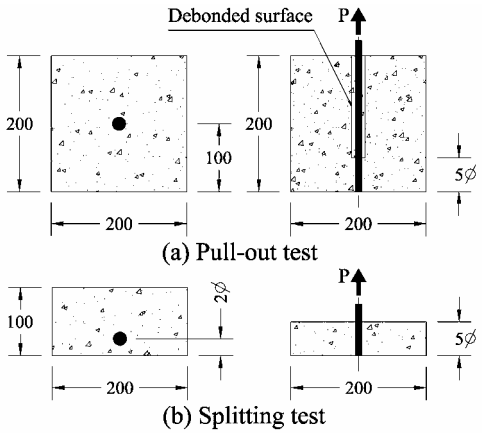

Figure 6. Concrete cubes and the configuration of the specimens.

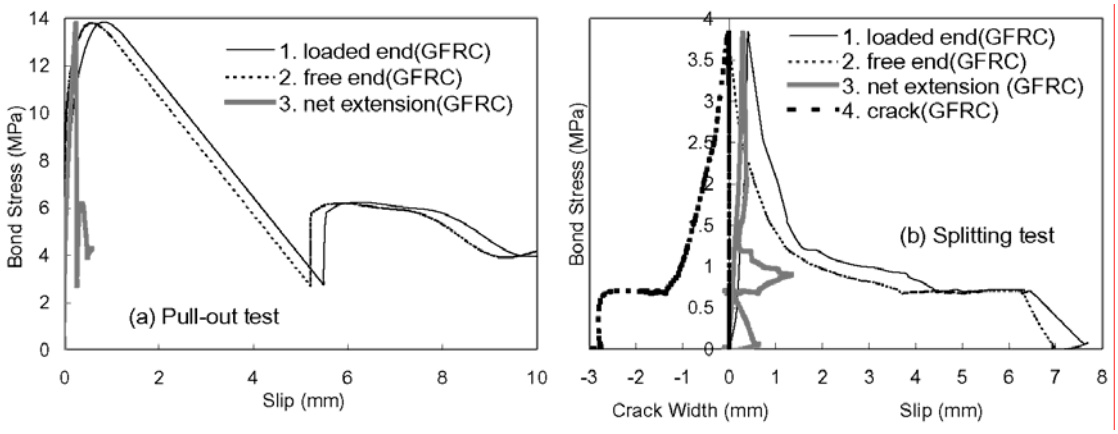

Figure 7. Bond stress–slip response in GFRC (8mm GFRP bar)

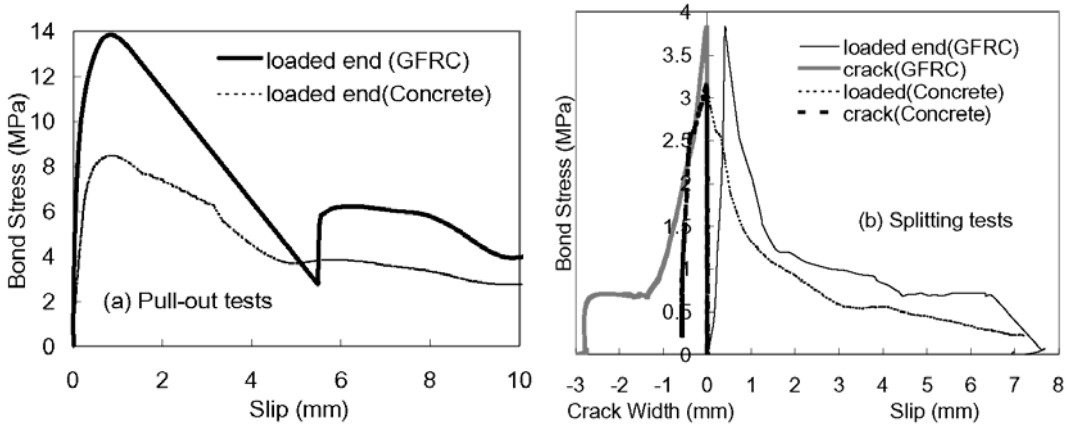

Figure 8. Bond stress–slip response in GFRC in GFRC and Concrete (8mm GFRP bar)

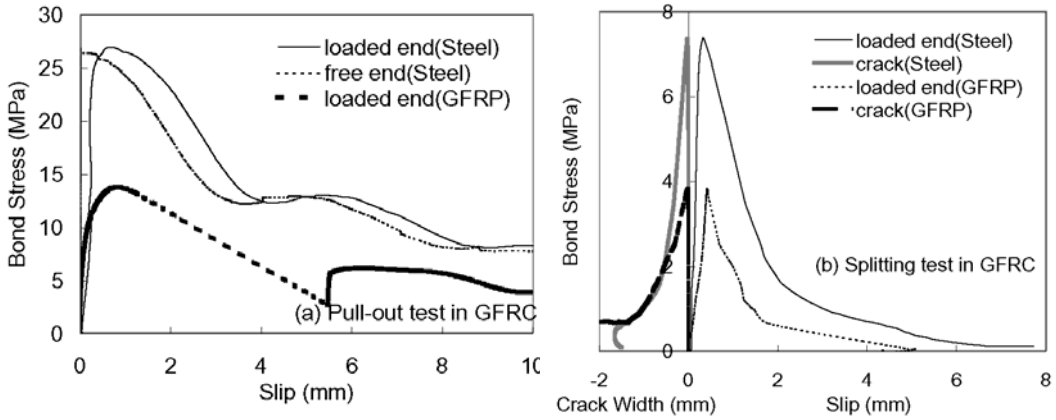

Figure 9. Pull-out stress & slip response (comparison of Steel and GFRP)

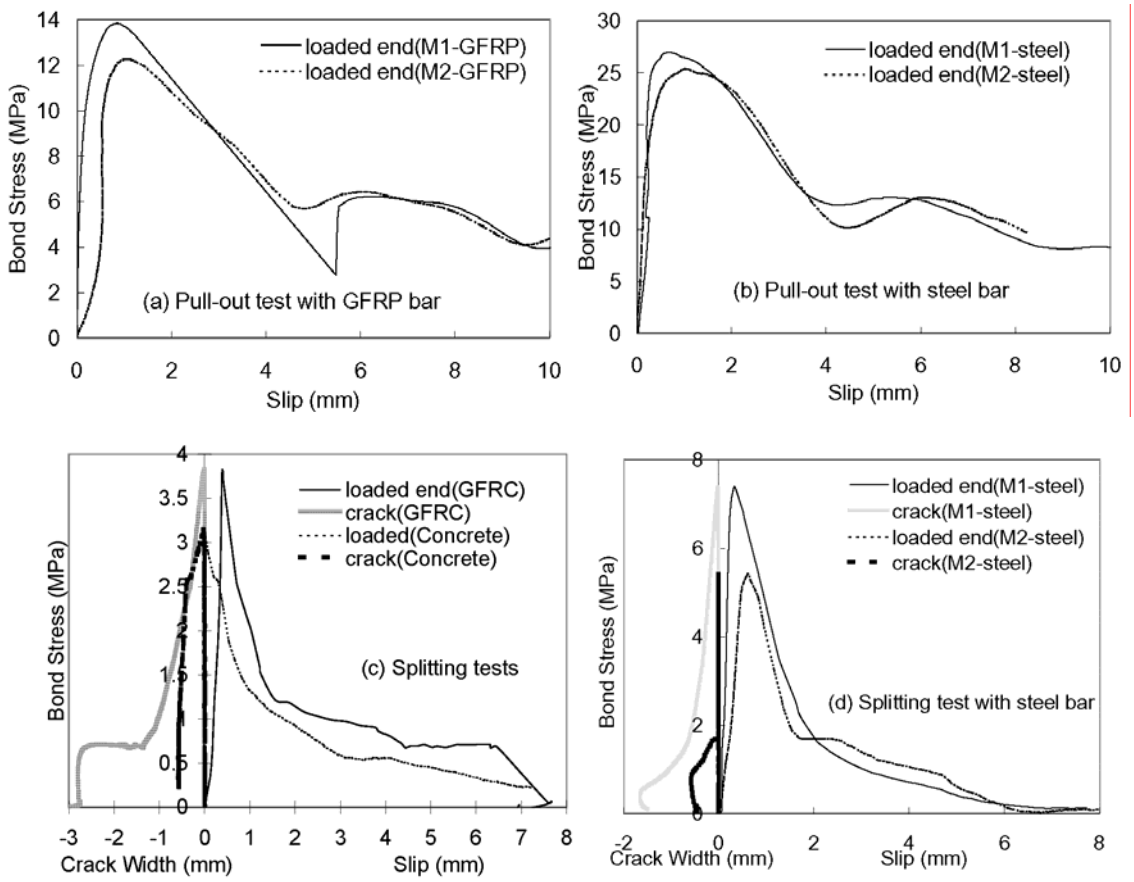

Figure 10. Pull-out stress & slip response (comparison of Mix 1 and Mix 2 with both 6mm steel bar & 8mm GFRP bar).

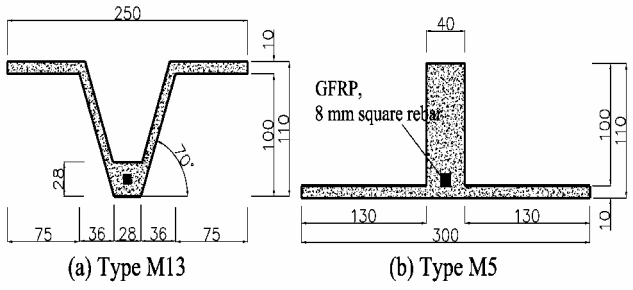

Figure 11. Typical FRP reinforced GFRC section

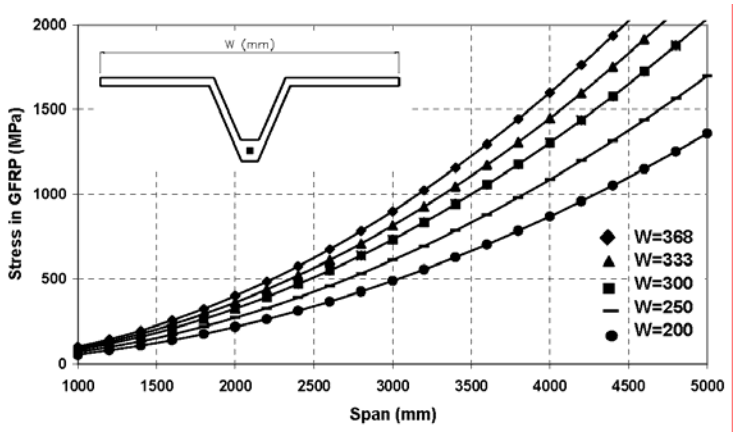

Figure 12. Stress in GFRP (Type M13 - reinforced)

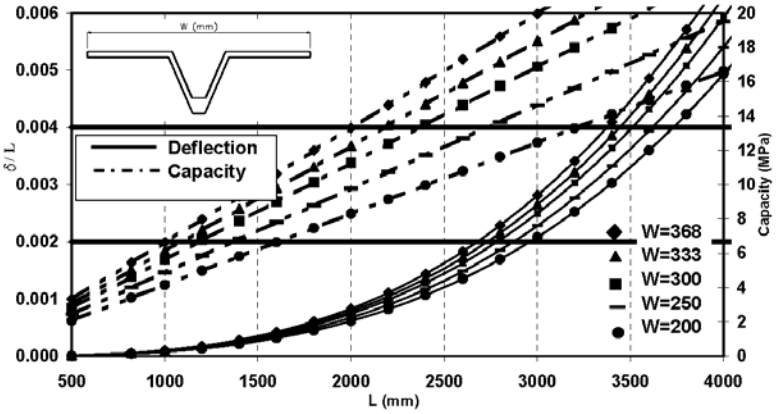

Figure 13. Deflection and capacity (Type M13 - unreinforced)

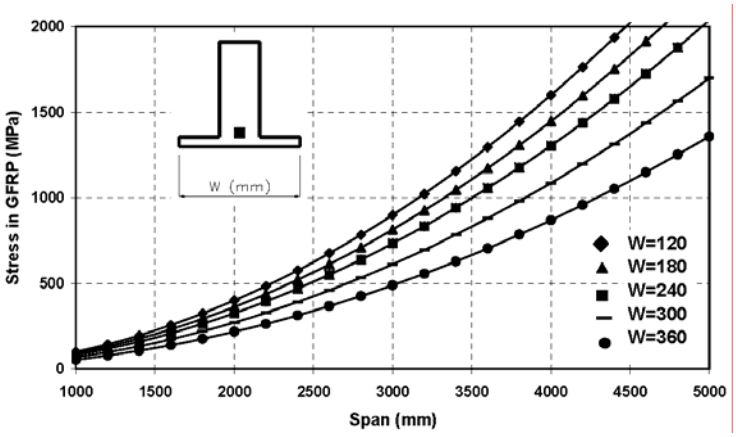

Figure 14. Stress in GFRP (Type M5 - reinforced)

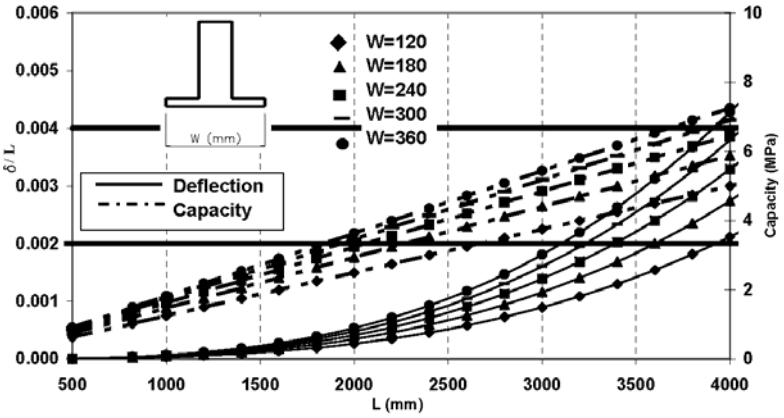

Figure 15. Deflection and capacity (Type M5 - unreinforced)

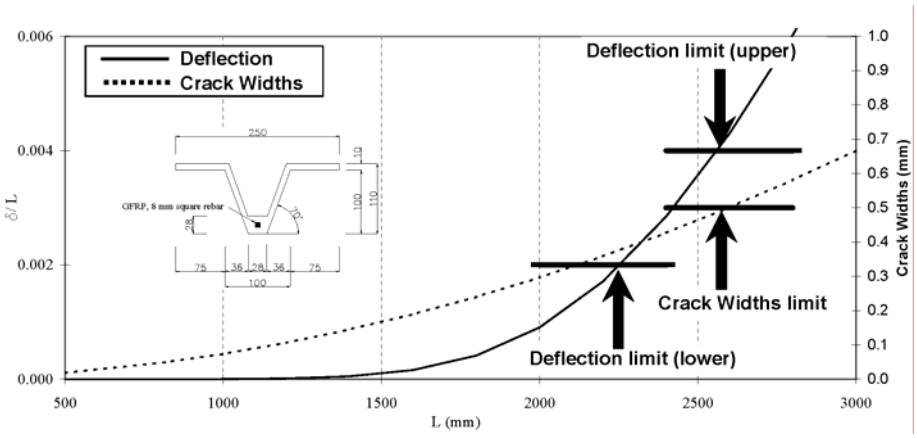

(a) Type M13

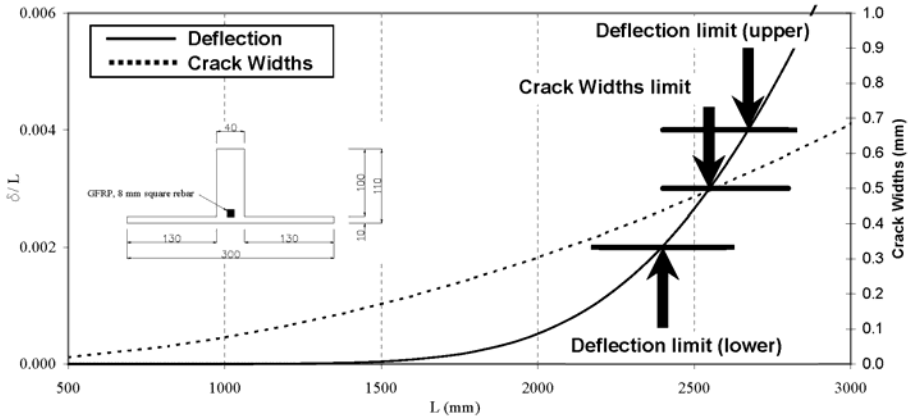

(b) Type M5

Figure 16. Deflection and crack widths over typical FRP reinforced GFRC section

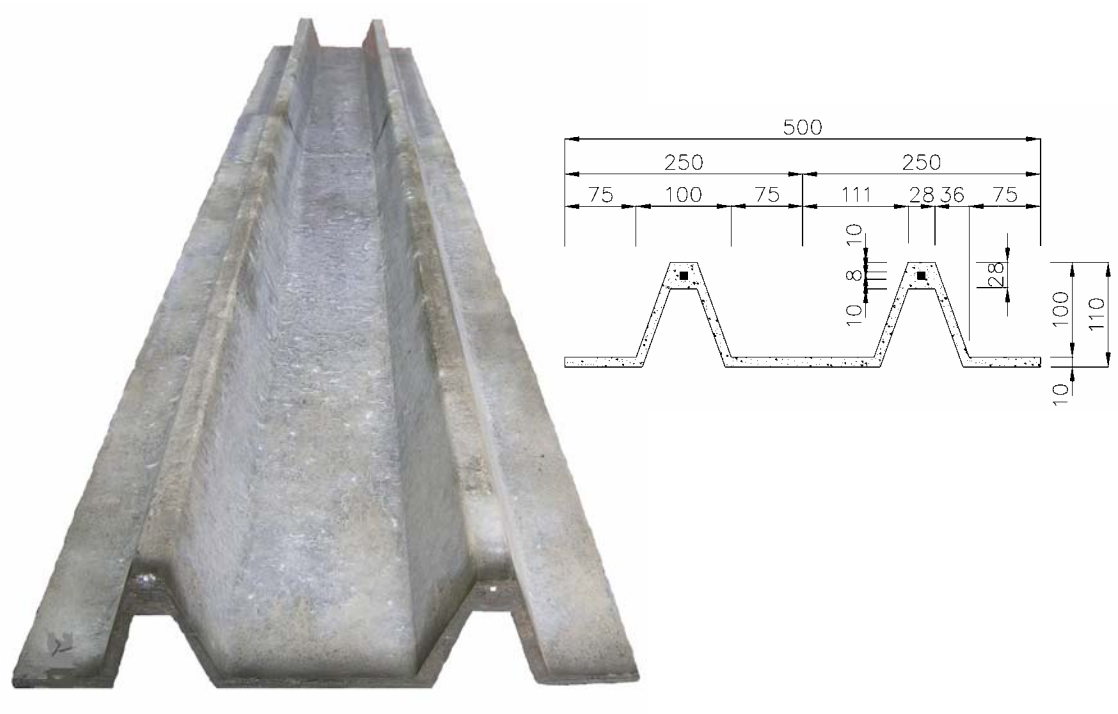

Figure 17. Testing specimen

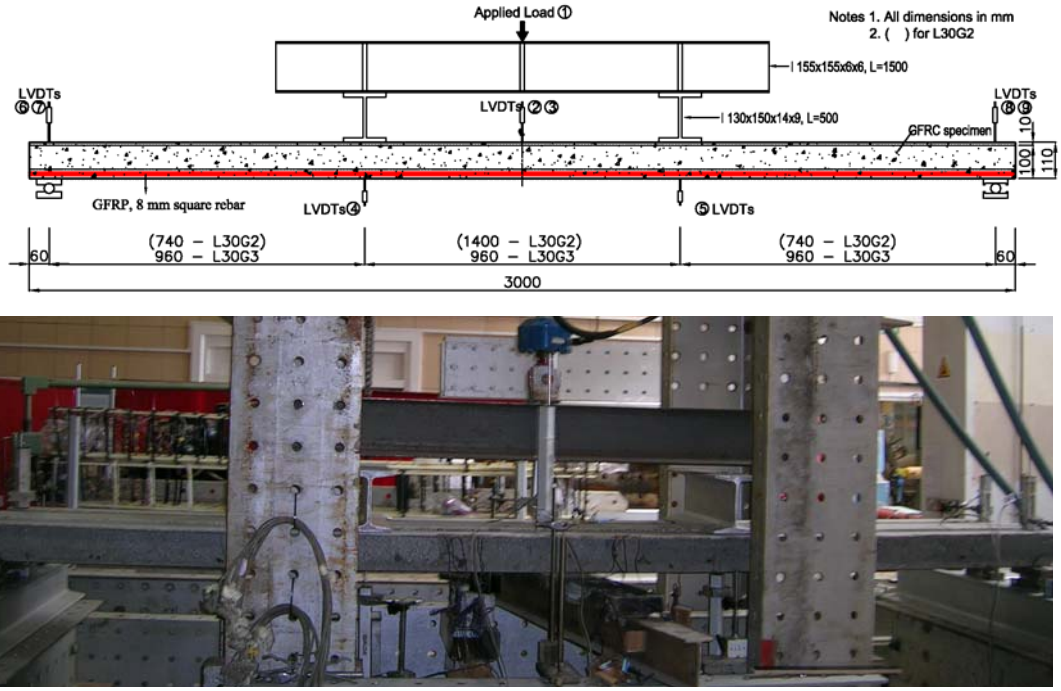

Figure 18. Instrumentation and measurement points on panel L30G3 and L30G2

Figure 19. After testing

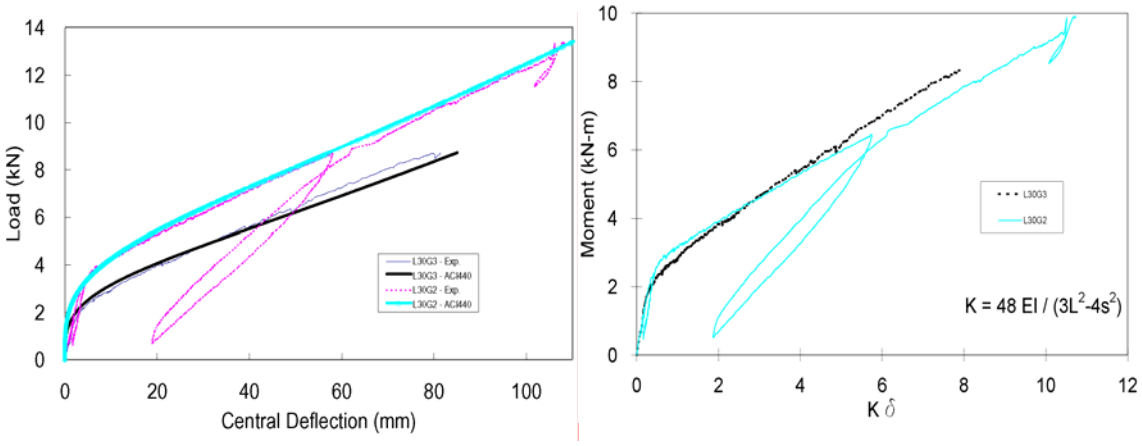

(a) load-deflection (b) moment resist

Figure 20. The average measured load-deflection and moment resist relationships for L30G3 and L30G2

List of Tables:

LIST OF FIGURE CAPTIONS